II International Conference on Particle-based Methods - Fundamentals and Applications
PARTICLES 2011
E. Oñate and D.R.J. Owen (Eds)

MESHFREE LARGE DEFORMATION ANALYSIS WITH MODIFIED FORMULATION OF FLOATING STRESS-POINT INTEGRATION

YUKI ONISHI*, KENJI AMAYA*, and Ryuta IMAI†

* Department of Mechanical and Environmental Informatics,
Tokyo Institute of Technology, Tokyo 152-8552, Japan
e-mail: yonishi@a.mei.titech.ac.jp, http://www.a.mei.titech.ac.jp/

† Mizuho Information & Research Institute, Inc., Tokyo 101-8443, Japan

Key words: Galerkin Meshfree Method, Moving Least Squares, Stress-point Integration, Large Deformation, Incremental Internal Force

Abstract. A modified formulation of floating stress-point integration for large deformation analysis is presented. The modified formulation introduces an incremental internal force to the equilibrium equation instead of the virtual external force introduced in our previous formulation. With this modification, the temporal continuity of the mechanical equilibrium can be kept without introducing the virtual external force, and thus the accumulating error due to time advancing becomes small compared to our previous formulation. A few examples of large deformation analysis are also presented to show the validity and accuracy of the proposing method in comparison with the finite element method.

1 INTRODUCTION

Galerkin meshfree methods are expected to be effective numerical methods for solid mechanics problems that are difficult to be analyzed by finite element methods (FEM). One of such problems is large deformation problem that induces several hundred percent of strain[1]. Adaptive meshing techniques sometimes can help convergent capability of FEM, but are not widely used due to their complexity and imperfections. Accordingly, large deformation problems such as forming processes are competent application of meshfree methods.

Traditional Galerkin meshfree methods such as element-free Galerkin method (EFGM)[2] require background cells for integration over the analysis domain. The integration with background cells, however, has a difficulty in transportation of history-dependent states such as plastic strain, viscous strain, and total strain without numerical dispersion in

large deformation analysis. There are mainly two types of solution to the difficulty[1]: nodal integration and stress-point integration. Nodal integration methods[3, 4, 5, 6] have a common problem that numerical oscillation of zero-energy modes arises without artificial stabilization terms. Stress-point integration methods for large deformation problems were studied by only a few[7, 8, 9], and the details of the formulation and quantitative performance evaluation haven't been shown so far.

We previously proposed a type of stress-point integration method named floating stress-point integration[11] and presented its formulation and examples of analysis. The previous formulation, however, has to introduce a virtual external force to enforce the temporal continuity of the mechanical equilibrium. Being a cause of error increasing over time, the virtual external force is problematic in terms of accuracy in highly large deformation cases.

In this study, a modified formulation of floating stress-point integration is presented. The modified formulation adopts the equilibrium equation in the incremental form instead of the total form. With this modification, the temporal continuity of the mechanical equilibrium can be kept without introducing the virtual external force, and thus the accumulating error due to time advancing becomes small compared to our previous formulation. In addition, the way of stress-point generation and support radius determination are slightly modified. The detail of modified formulation of the proposing method and a few examples of large deformation analysis are presented in this paper.

2 CONSTITUTIVE EQUATIONS

For the large deformation of isotropic elastic bodies, we adopt the following elastic constitutive equations:

$$\boldsymbol{T} = \boldsymbol{C} : \boldsymbol{E} \quad (\text{i.e., } \mathring{\boldsymbol{T}} = \boldsymbol{C} : \boldsymbol{D}), \tag{1}$$

where $\boldsymbol{T}$ is the Cauchy stress tensor, $\boldsymbol{E}$ is the Hencky strain tensor, $\mathring{\boldsymbol{T}}$ is the Jaumann rate of the Cauchy stress, $\boldsymbol{D}$ is the stretching tensor, and $\boldsymbol{C}$ is the 4th order elasticity tensor described as the following.

$$C_{ijkl} = \lambda \delta_{ij} \delta_{kl} + 2\mu \delta_{ik} \delta_{jl}, \tag{2}$$

where λ and μ are the Lame's parameters.

3 FORMULATIONS OF THE PROPOSING METHOD

For the sake of simplicity, we describe the proposing formulation for homogeneous material under two-dimensional plane strain quasi-static condition. Note that the presenting formulation can be easily extended to the formulation of heterogeneous material under three-dimensional condition.

In this section, variables defined at a stress-point I are denoted with the superscript I to the left of the variables. In a similar fashion, variables defined at a node J are denoted

with the subscript J to the left of the variables. Also, trial variables of time increments are denoted with the superscript $+$ to the right of the variables.

The flowchart of the proposing method is shown in Fig.1 in advance. The following subsections in this section present the detail of each process of the flowchart.

3.1 Spacial Discretization and Initialization

Figure 2 shows the outline of the spacial discretization method in this study. The initial analysis domain is discretized into unstructured meshes with coarseness and fineness. The vertices defining the cells are treated as nodes, while stress-points are systematically generated in the cells and on the edges. Each stress-point I holds its initial corresponding volume, ${}^{I}V^{\mathrm{ini.}}$, for the domain integration described later. Note that the cells and the edges are used only for the initialization of the nodes and stress-points and are never

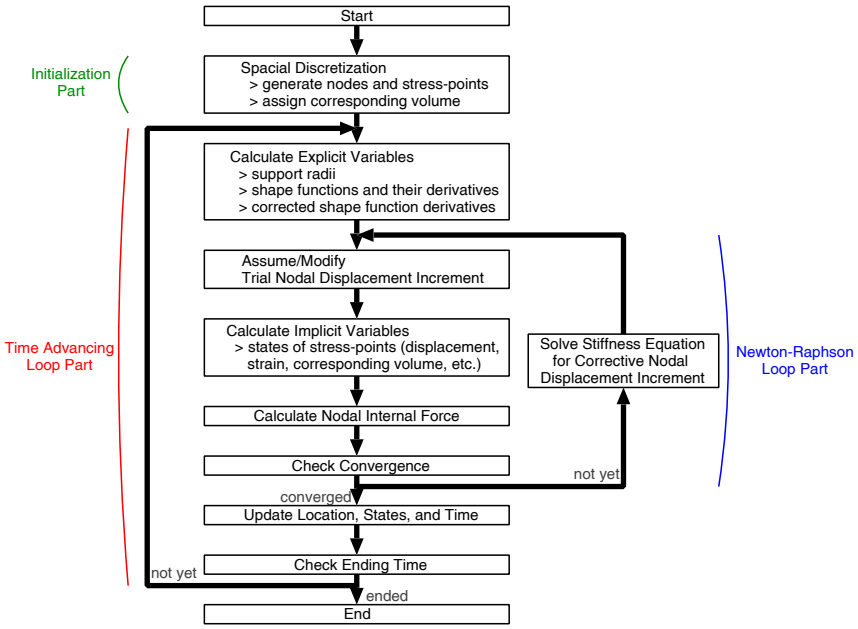

Figure 1: Flowchart of the proposing meshfree method. The detail of each process is described in §3.

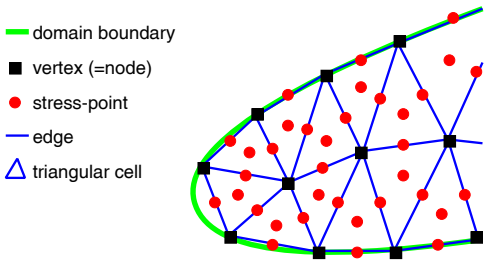

Figure 2: Outline of spacial discretization of the present method in two-dimensional cases. The cells are used only at the initial state and are never referred during the time advancing steps.

referred during the time advancing steps.

In case of two-dimensional problems, the analysis domain is discretized into triangular meshes. Stress-points are generated at the center of each cell and at the center of each edge. The ${}^{I}V^{\text{ini.}}$ are assigned as

$$ {}^{I}V^{\text{ini.}} = \begin{cases} \frac{1}{4}V_I & (\text{if } I \text{ is in a cell}) \\ \frac{1}{4}V_{I_A} + \frac{1}{4}V_{I_B} & (\text{if } I \text{ is on an edge}) \end{cases}, \tag{3} $$

where V_I is the volume of the cell including the stress-point I, V_{I_A} and V_{I_B} are the volumes of the cells pinching the stress-point I. The sum of ${}^{I}V^{\text{ini.}}$ for all stress-points is equal to the volume of initial analysis domain.

The way of stress-point generation and corresponding volume distribution proposed here is not an optimal one but just an example. Optimization of the way is an issue in the future.

3.2 Shape Function and Its Derivatives

For the approximation of spacial variables, moving-least-square (MLS) approximation method[2] was employed. The polynomial basis used in this study is the 1st order polynomial basis given by

$$ \{p(\boldsymbol{x})\} = \{1,\ x_1,\ x_2\}, \tag{4} $$

where $\boldsymbol{x}$ is the coordinates in the Cartesian space, $\{x_1,\ x_2\}^T$. For simplicity, the basis at a stress-point I or a node J are written as follows, respectively, later in this paper.

$$ \{{}^{I}p\} = \{p({}^{I}\boldsymbol{x})\}, \quad \{{}_{J}p\} = \{p({}_{J}\boldsymbol{x})\}. \tag{5} $$

The weight function defined as a function of a positive parameter d, $w(d)$, is given by

$$ w(d) = \begin{cases} \frac{1}{d} - 1 & (0 < d < 1) \\ 0 & (1 \leq d) \end{cases}. \tag{6} $$

The weight at a stress-point I for a node J, ${}^{I}_{J}w$, is defined as

$$ {}^{I}_{J}w = w\left(\frac{||{}_{J}\boldsymbol{x} - {}^{I}\boldsymbol{x}||}{{}^{I}R} \right), \tag{7} $$

where ${}^{I}R$ is the support radius varied with time and the location of I. The way to decide ${}^{I}R$ is described later.

The shape function at a stress-point I, $\{{}^{I}N\}$ $(= \{N({}^{I}\boldsymbol{x})\})$, is given by

$$ \{{}^{I}N\} = \{{}^{I}p\}\ [{}^{I}A]^{-1}\ [{}^{I}B], \tag{8} $$

where $[{}^{I}A]$ and $[{}^{I}B]$ are matrices defined as

$$[{}^{I}A] = \sum_{J \in {}^{I}\mathbb{J}} {}^{I}_{J}w \ \{{}_{J}p\}^{T}\{{}_{J}p\}, \tag{9}$$

$$[{}^{I}B] = \left[{}^{I}_{{}^{I}\mathrm{J}_1}w \ \{{}_{{}^{I}\mathrm{J}_1}p\}^{T}, \ {}^{I}_{{}^{I}\mathrm{J}_2}w \ \{{}_{{}^{I}\mathrm{J}_2}p\}^{T}, \ \cdots, \ {}^{I}_{{}^{I}\mathrm{J}_{|{}^{I}\mathbb{J}|}}w \ \{{}_{{}^{I}\mathrm{J}_{|{}^{I}\mathbb{J}|}}p\}^{T} \right], \tag{10}$$

where ${}^{I}\mathbb{J}$ is the node set in the support domain of I, ${}^{I}\mathrm{J}_k$ is the kth node member in ${}^{I}\mathbb{J}$, and $|{}^{I}\mathbb{J}|$ is the number of nodes in ${}^{I}\mathbb{J}$.

The partial derivatives of the shape function with respect to ${}^{I}x_i$, $\{{}^{I}N'_i\}$ $(= \frac{\partial\{{}^{I}N\}}{\partial {}^{I}x_i})$, can be calculated as follows:

$$\{{}^{I}N'_i\} = \left(\frac{\partial\{{}^{I}p\}}{\partial {}^{I}x_i}\right)[{}^{I}A]^{-1}[{}^{I}B] + \{{}^{I}p\}\left(\frac{\partial[{}^{I}A]^{-1}}{\partial {}^{I}x_i}\right)[{}^{I}B] + \{{}^{I}p\}[{}^{I}A]^{-1}\left(\frac{\partial[{}^{I}B]}{\partial {}^{I}x_i}\right), \tag{11}$$

where $\frac{\partial[{}^{I}A]^{-1}}{\partial {}^{I}x_i}$ is a matrix given by

$$\frac{\partial[{}^{I}A]^{-1}}{\partial {}^{I}x_i} = -[{}^{I}A]^{-1}\left(\frac{\partial[{}^{I}A]}{\partial {}^{I}x_i}\right)[{}^{I}A]^{-1}. \tag{12}$$

From now, the value of the shape function at a stress-point I for a node J is written as ${}^{I}_{J}N$. In addition, the vector consisting of spacial derivatives of ${}^{I}_{J}N$ is written as ${}^{I}_{J}\boldsymbol{N}'$.

3.3 Integration Correction

For the satisfaction of integration constraints[4] or divergence-free condition[10], which is an essential qualification to pass the patch tests, integration correction should be applied. In this study, integration correction is realized by the scaling type correction[13]:

$${}^{I}_{J}\widetilde{\boldsymbol{N}'} = (1 + {}^{I}\gamma)\ {}^{I}_{J}\boldsymbol{N}', \tag{13}$$

where ${}^{I}_{J}\widetilde{\boldsymbol{N}'}$ is the correction of ${}^{I}_{J}\boldsymbol{N}'$ and ${}^{I}\gamma$ is the correction coefficient independent from node J. Equations of integration constraints in the proposing formulation are given by

$$\sum_{I \in {}_{J}\mathbb{I}} {}^{I}_{J}\widetilde{\boldsymbol{N}'}{}^{I}V = \boldsymbol{0} \qquad \text{(for } J \text{ in interior nodes)}, \tag{14}$$

$$\sum_{I \in {}_{J}\mathbb{I}} {}^{I}_{J}\widetilde{\boldsymbol{N}'}{}^{I}V - {}_{J}\boldsymbol{n}\,{}_{J}A = \boldsymbol{0} \qquad \text{(for } J \text{ in exterior nodes)}, \tag{15}$$

where ${}_{J}\mathbb{I}$ is the set of stress-points such that have J in their support domain, ${}_{J}\boldsymbol{n}$ is the nodal outward unit normal vector, and ${}_{J}A$ is the nodal corresponding surface area. Substituting Eq.(13) into the Eqs.(14) and (15), we obtain the following simultaneous equation in the matrix form:

$$[\mathcal{N}']\{\gamma\} = \{\mathcal{R}\}, \tag{16}$$

where $[\mathcal{N}']$ is the left-hand side matrix consisting of ${}_J^I\boldsymbol{N}'$s, $\{\gamma\}$ is the left-hand side unknown vector consisting of ${}^I\gamma$s, and $\{\mathcal{R}\}$ is right-hand side known vector consisting of residuals. Since the number of stress-points is greater than the number of nodes, Eq.(16) is an underdetermined system. In this study, we simply took the minimum norm solution as $\{\gamma\}$.

3.4 Quasi-implicit Time Advancing

Focusing on the highly large deformation analysis, the proposing method adopts the updated-Lagrangian approach. For the fully implicit time advancing with the updated-Lagrangian approach, update of the support, weight, and shape function of each stress-point is necessary in every convergent calculation of the backward difference. This update, however, causes difficulty of convergence.

We introduced a quasi-implicit time advancing scheme to overcome the difficulty of the fully implicit time advancing. In this scheme, variables to be updated are separated into two types, explicit variables and implicit variables, as follows.

3.4.1 Explicit Variables

The support radius, the weight, the shape function, and its derivatives for each stress-point are treated as explicit variables, which are updated before the starts of the Newton-Raphson loop in Fig.1. Thus these explicit variables are kept constant within each Newton-Raphson loop.

The support radius for a stress-point I, ${}^IR$, is set to be a minimum value under the following required conditions:

· The number of nodes in the support is 6 or more ($|{}^I\mathbb{J}| \geq 6$),

· The condition number of $[{}^IA]$ defined in Eq.(9) is less than 10^5 ($\mathrm{cond}([{}^IA]) < 10^5$).

In the actual implementation, ${}^IR$ is initialized as a small value and multiplied by 1.01 iteratively until the conditions above are satisfied. This way to set ${}^IR$ can avoid breakdowns of shape function construction in cases of non-uniform or irregular distribution of nodes. The other explicit variables are calculated as described in §3.2.

3.4.2 Implicit Variables

State variables of stress-points except the explicit variables are treated as implicit variables. The trial position of a stress-point I, ${}^I\boldsymbol{x}^+$, is updated by

$$ {}^I\boldsymbol{x}^+ = {}^I\boldsymbol{x} + \sum_{J\in{}^I\mathbb{J}} {}_J^IN \ ({}_J\boldsymbol{x}^+ - {}_J\boldsymbol{x}), \tag{17} $$

where ${}_J\boldsymbol{x}^+$ is the trial position of a node J. The trial corresponding volume of a stress-point I, ${}^IV^+$, is updated by

$$ {}^IV^+ = {}^IV^{\mathrm{ini.}}\det({}^I\boldsymbol{F}^+), \tag{18} $$

where ${}^{I}\boldsymbol{F}^{+}$ is the trial total deformation gradient tensor. Other implicit variables of stress-points are calculated in the same fashion as the standard FEM[12].

3.5 Virtual Work Equation and Equilibrium Equation

One kind of form of the virtual work equation for solid mechanics[14] excluding the body force term is written as

$$\int_v \dot{\boldsymbol{\Pi}}_t^T(t) : \delta \boldsymbol{F}_t(t)\ \mathrm{d}v = \int_s \dot{\underline{\boldsymbol{t}}}_t(t) \cdot \delta \boldsymbol{u}\ \mathrm{d}s, \tag{19}$$

where v is the current volume, s is the current boundary, "$\dot{}$" denotes the material time derivatives, $\boldsymbol{\Pi}_t(t)$ is the first Piola-Kirchhoff stress tensor in the current configuration, $\delta \boldsymbol{F}_t(t)$ is the variation of the deformation gradient tensor in the current configuration, $\underline{\boldsymbol{t}}_t(t)$ is the surface traction vector in the current configuration, and $\delta \boldsymbol{u}$ is the variation of the displacement vector. Through the linear approximation of material time derivatives during an increment, $\dot{\boldsymbol{\Pi}}_t^T(t)$ and $\dot{\underline{\boldsymbol{t}}}_t(t)$ can be approximated as $\Delta\boldsymbol{\Pi}_t^{T+}$ and $\Delta\underline{\boldsymbol{t}}_t$, respectively. By applying the Galerkin method to the proposed spacial discretization, $\delta \boldsymbol{u}$ and $\delta \boldsymbol{F}_t(t)$ can be discretized as $\{N\}\{\delta u\}$ and $[B_{\mathrm{N}}]\{\delta u\}$, respectively, where $\{\delta u\}$ is the variation of nodal displacement and $[B_{\mathrm{N}}]$ is a matrix consisting of $\widetilde{\boldsymbol{N}}'$s. Consequently, the following discretized equilibrium equation in incremental form is obtained.

$$\{\Delta f^{\mathrm{ext.}+}\} - \{\Delta f^{\mathrm{int.}+}\} = \{0\}, \tag{20}$$

where $\{\Delta f^{\mathrm{ext.}+}\}$ is the nodal external force vector increment and $\{\Delta f^{\mathrm{int.}+}\}$ is the nodal internal force vector increment given by

$$\{\Delta f^{\mathrm{int.}+}\} = \sum_{I\in\mathbb{I}_\Omega} \int_{{}^{I}\Omega} [\widetilde{B}_{\mathrm{N}}]^T \{\Delta\Pi_t^{T+}\}\ \mathrm{d}\Omega \simeq \sum_{I\in\mathbb{I}_\Omega} [{}^{I}\widetilde{B}_{\mathrm{N}}]^T \{\Delta {}^{I}\Pi_t^{T+}\} {}^{I}V^{+}, \tag{21}$$

$$[{}^{I}\widetilde{B}_{\mathrm{N}}] = \begin{bmatrix} {}^{I}_{\mathrm{J}_1}\widetilde{N'}_1 & 0 & \cdots & {}^{I}_{\mathrm{J}_{|I_{\mathbb{J}}|}}\widetilde{N'}_1 & 0 \\ 0 & {}^{I}_{\mathrm{J}_1}\widetilde{N'}_2 & \cdots & 0 & {}^{I}_{\mathrm{J}_{|I_{\mathbb{J}}|}}\widetilde{N'}_2 \\ {}^{I}_{\mathrm{J}_1}\widetilde{N'}_2 & 0 & \cdots & {}^{I}_{\mathrm{J}_{|I_{\mathbb{J}}|}}\widetilde{N'}_2 & 0 \\ 0 & {}^{I}_{\mathrm{J}_1}\widetilde{N'}_1 & \cdots & 0 & {}^{I}_{\mathrm{J}_{|I_{\mathbb{J}}|}}\widetilde{N'}_1 \end{bmatrix}, \tag{22}$$

$$\Delta {}^{I}\boldsymbol{\Pi}_t^{+} = \Delta {}^{I}\boldsymbol{T}^{+} - {}^{I}\boldsymbol{T}\left(({}^{I}\boldsymbol{L}^{+}\Delta t)^T - \mathrm{tr}({}^{I}\boldsymbol{L}^{+}\Delta t)\boldsymbol{I}\right), \tag{23}$$

where $\boldsymbol{L}$ and $\boldsymbol{I}$ are velocity gradient tensor and identity tensor, respectively. Since $\Delta {}^{I}\boldsymbol{\Pi}_t^{+}$ approaches to $\boldsymbol{0}$ as Δt approaches to $+0$, the left-hand side of Eq.(20) is also approaches to $\boldsymbol{0}$ as Δt approaches to $+0$. Thus, Eq.(20) is always satisfied on the condition of $\Delta t = 0$ regardless of the update of the support before the start of the Newton-Raphson loop; the temporal continuity of the mechanical equilibrium between time increments is always achieved.

The way of stiffness equation construction and the way of boundary condition treatment are in the same fashion as standard FEM[12].

4 EXAMPLES OF ANALYSIS

For the accuracy verification of the proposing method, a few examples of analysis in plane strain condition are shown in this section. Commercial finite element software, ABAQUS/Standard[15], are used to make reference solutions.

4.1 Cantilever Bending Analysis

Figure 3 shows the initial analysis domain and locations of nodes and stress-points for the cantilever bending analysis. The domain is a 0.1 m×1 m rectangular. The number of nodes, initializing cells, and stress-points are 335, 558, and 1450, respectively. The material of the domain is an elastic material of 1 GPa Young's modulus and 0.3 Poisson's ratio, i.e. $\lambda = 0.576923$ GPa and $\mu = 0.384615$ GPa. The left side nodes were geometrically constrained, and 400 kN concentrated force was applied to the top-right node toward the vertical downward direction. The analysis time span was discretized into 198 unequal time steps with automatic time step control. The solution of this problem using ABAQUS/Standard with 1000 (=10×100) 2nd-order quadrilateral elements and 1000 equal time steps is prepared as a reference solution.

Figure 4 shows the deformed shape and Mises stress distribution in the final state. Figure 5 shows the relation between the applied vertical force and the vertical displacement at the top-right node. The displacement error of the proposing method is less than 0.3%. Thorough this analysis, it was confirmed that the proposing method can avoid the shear locking and has enough accuracy to solve large deflection analyses.

Figure 3: Initial locations of nodes (gray dots) and stress-points (blue dots) for the cantilever example

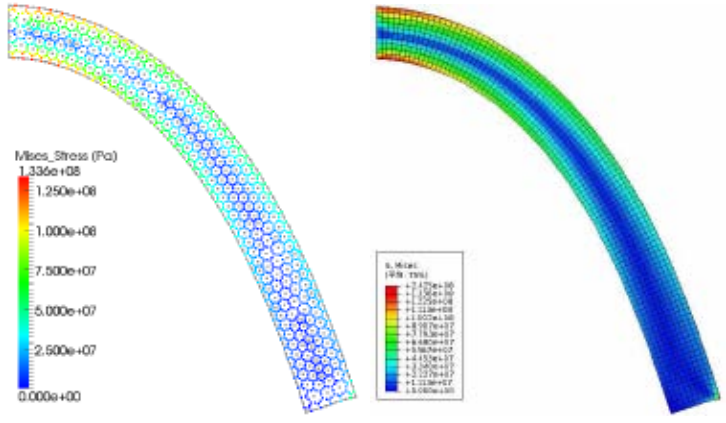

Figure 4: Deformed shape and Mises stress distribution in the final state of the cantilever example with the proposing method (left) and ABAQUS/Standard (right).

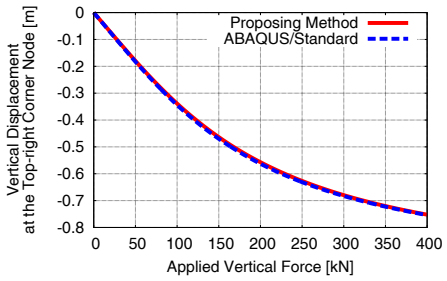

Figure 5: Comparison of vertical displacement at the loading point (top-right corner node) of the cantilever example between the proposing method and ABAQUS/Standard.

4.2 Uniaxial Tension Analysis

Figure 6 shows the initial analysis domain and locations of nodes and stress-points for the uniaxial tension analysis. The domain is a 1 m×1 m rectangular with a quarter circular hole of 0.8 m radius. The number of nodes, initializing cells, and stress-points are 873, 1,598, and 4,068, respectively. The material properties are the same as the previous example. The left side nodes were horizontally constrained; the bottom side nodes were vertically constrained; the top side nodes were horizontally constrained and displaced 1 m toward the vertical upward direction. The analysis time span was discretized into 352 unequal time steps with the automatic time step control. The solution of this problem using ABAQUS/Standard with 1,598 1st-order triangular elements meshed as the initializing cells and the automatic time step control is prepared as a reference solution.

Figure 7 shows the deformed shape and Mises stress distribution at the moment of 0.5 m displacement. Figure 8 shows the deformed shape and Mises stress distribution in the final

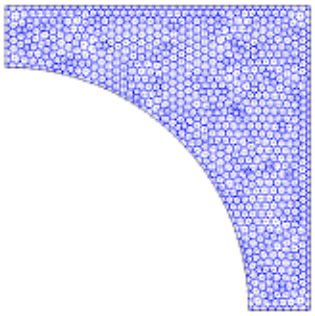

Figure 6: Initial locations of nodes (gray dots) and stress-points (blue dots) for the uniaxial tension analysis.

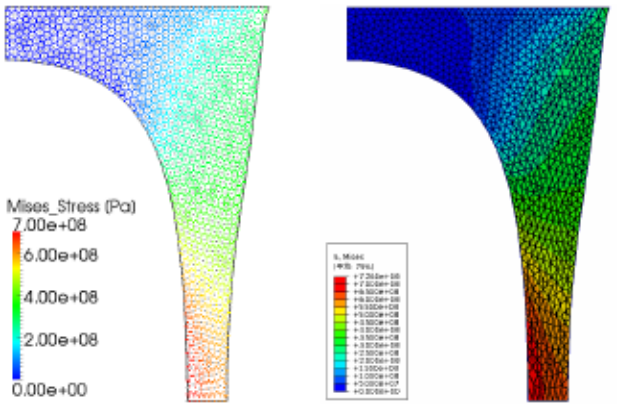

Figure 7: Deformed shape and Mises stress distribution at the moment of 0.5 m displacement of the uniaxial tension analysis with the proposing method (left) and ABAQUS/Standard (right).

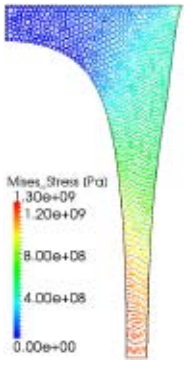

Figure 8: Deformed shape and Mises stress distribution at the moment of 1 m displacement of the uniaxial tension analysis with the proposing method.

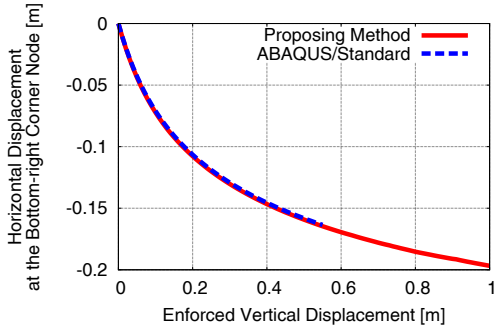

Figure 9: Comparison of horizontal displacement at the bottom-right corner node of the uniaxial tension example between the proposing method and ABAQUS/Standard.

state (1 m displacement) with the proposing method, while that with ABAQUS/Standard was not obtained because of excessive distortion and volumetric locking of elements. Figure 9 shows the relation between the enforced displacement and the horizontal displacement at the bottom-right node. As the displacement error of the proposing method is less than 1% until the limit of ABAQUS/Standard, the result of proposing method in the final state is expected to be appropriate.

4.3 Uniaxial Compression Analysis

Figure 10 shows the initial analysis domain and locations of nodes and stress-points for the uniaxial compression analysis. The domain is a 1 m×0.5 m rectangular. The number of nodes, initializing cells, and stress-points are 528, 964, and 2,455, respectively. The material of the domain is an elastic material of 1 GPa Young's modulus and 0.45 Poisson's ratio, i.e. $\lambda = 3.103448$ GPa and $\mu = 0.3448276$ GPa. The left side nodes were horizontally constrained; the bottom side nodes were vertically constrained; the top side

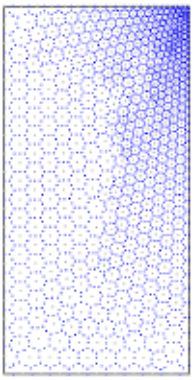

Figure 10: Initial locations of nodes (gray dots) and stress-points (blue dots) for the uniaxial compression example.

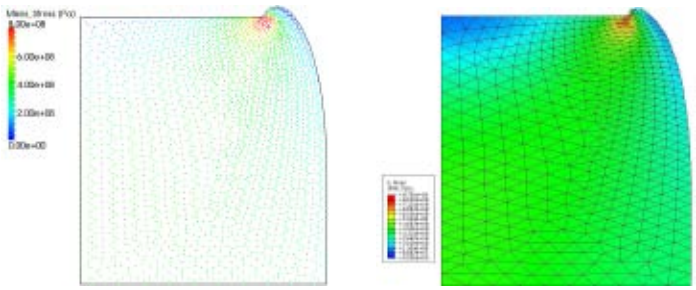

Figure 11: Deformed shape and Mises stress distribution at the moment of 0.28 m displacement of the uniaxial compression example with the proposing method (left) and ABAQUS/Standard (right).

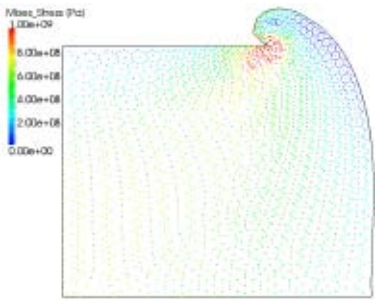

Figure 12: Deformed shape and Mises stress distribution at the moment of 0.4 m displacement of the uniaxial compression example with the proposing method.

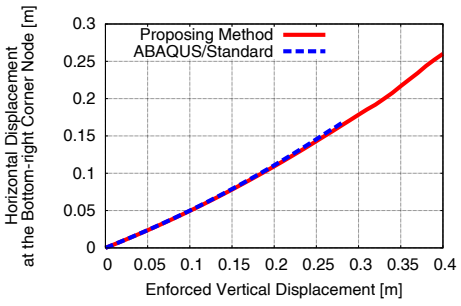

Figure 13: Comparison of horizontal displacement at the bottom-right corner node of the uniaxial compression example between the proposing method and ABAQUS/Standard.

nodes were horizontally constrained and displaced 0.4 m toward the vertical downward direction. The analysis time span was discretized into 611 unequal time steps with the automatic time step control. The solution of this problem using ABAQUS/Standard with 964 1st-order triangular elements meshed as the initializing cells and the automatic time step control is prepared as a reference solution.

Figure 11 shows the deformed shape and Mises stress distribution at the moment of 0.28 m displacement. Figure 12 shows the deformed shape and Mises stress distribution in the final state (0.4 m displacement) with the proposing method, while that with ABAQUS/Standard was not obtained because of excessive distortion of elements. Figure 13 shows the relation between the enforced displacement and the horizontal displacement at the bottom-right node. The displacement error of the proposing method is less than 3% until the limit of ABAQUS/Standard. A few stress-points around the top-right corner, however, squeezed out of the analysis domain. Improvement of the update scheme of stress-point positions as prescribed in Eq.(18) is an issue to be resolved.

5 CONCLUSIONS

A modified formulation of floating stress-point integration for large deformation analysis was presented. The modified formulation based on the virtual work equation in the rate form introduces an incremental internal force to the equilibrium equation instead of the virtual external force introduced in our previous formulation. A scaling type integration correction was adopted so that the proposed method satisfied the divergence-free condition and passed patch tests. A quasi-implicit time advancing scheme was introduced to avoid both the convergence difficulty of the fully implicit scheme and the accumulating error of the fully explicit scheme.

Several examples of large deformation analysis were presented to show the validity and accuracy of the proposed method. The results of the proposed method agreed with those of ABAQUS/Standard within the range of ABAQUS/Standard gave the solution and seemed appropriate out of that range. Further improvements of stress-point arrangement and location update of stress-points will make the proposed method to be much stable and accurate. After these improvements, development of contact functions, and implementation of mixed formulations for nearly incompressible material etc., it would be expected that the proposed method could be an effective numerical method for practical large deformation analysis.

REFERENCES

[1] S. Li and W. K. Liu, “Meshfree and particle methods and their applications”, *Applied Mechanics Reviews*, Vol. 55, No. 1, (2002), pp. 1–34

[2] T. Belytschko, Y. Y. Lu, and L. Gu, “Element-free Galerkin methods”, *International Journal for Numerical Methods in Engineering*, Vol. 37, (1994), pp. 229–256

[3] S. Beissel and T. Belytschko, "Nodal integration of the element-free Galerkin method", *Computer Methods in Applied Mechanics and Engineering*, Vol. 139, (1996), pp. 49–74

[4] J. S. Chen, C. T. Wu, S. Yoon, and Y. You, "A stabilized conforming nodal integration for Galerkin mesh-free methods", *International Journal for Numerical Methods in Engineering*, Vol. 50, (2001), pp. 435–466

[5] J. S. Chen, S. Yoon, and C. T. Wu, "Non-linear version of stabilized conforming nodal integration for Galerkin mesh-free methods", *International Journal for Numerical Methods in Engineering*, Vol. 53, (2002), pp. 2587–2615

[6] M. A. Puso, J. S. Chen, E. Zywicz, and W. Elmer, "Meshfree and finite element nodal integration methods", *International Journal for Numerical Methods in Engineering*, Vol. 74, (2008), pp. 416–446

[7] G. Li and T. Belytschko, "Element-free Galerkin method for contact problems in metal forming analysis", *Engineering Computations*, Vol. 18, No. 1/2, (2001), pp. 62–78

[8] Q. Duan and T. Belytschko, "Gradient and dilatational stabilizations for stress-point integration in the element-free Galerkin method", *International Journal for Numerical Methods in Engineering*, Vol. 77, (2009), pp. 776–798

[9] P. W. Randles and L. D. Libersky, "Normalized SPH with stress points", *International Journal for Numerical Methods in Engineering*, Vol. 48, (2000), pp. 1445–1462

[10] Y. Krongauz and T. Belytschko, "Consistent pseudo-derivatives in meshless methods", *Computer Methods in Applied Mechanics and Engineering*, Vol. 146, (1997), pp. 371–386

[11] Y. Onishi and K. Amaya, "A Novel Meshfree Method for Large Deformation Analysis of Elastic and Viscoelastic Bodies without using Background Cells", *Journal of Solid Mechanics and Materials Engineering*, Vol. 4, No. 11 (2010), pp.1673–1686

[12] O. C. Zienkiewicz, *The Finite Element Method for Solid and Structural Mechanics 6th Ed.*, (2005), Elsevier

[13] G. R. Liu, *Meshfree Methods 2nd Ed.*, (2010), CRC Press

[14] T. Hisada and H. Noguchi, *Basis and Application of Non-linear Finite Element Method* (in Japanese), (1995), Maruzen

[15] SIMULIA Inc., *ABAQUS 6.8 Documentation*, (2008), SIMULIA